Enhancing magnetic separation of nanoparticles

Pavel Kuzhir, Hinda Ezzaier, Jessica A Marins, Cécilia Magnet, Yaroslova Izmaylov, Cyrille Claudet

Enhancing magnetic separation of nanoparticles

Pavel Kuzhir, Hinda Ezzaier, Jessica A. Marins,
Cécilia Magnet, Yaroslova Izmaylov, Cyrille Claudet

Abstract This paper briefly reviews our recent advances in the magnetic separation of nanoparticles, which has long been considered challenging because of their strong Brownian motion. We show that field-induced phase separation enhances significantly the efficiency of nanoparticle magnetic separation that is expected to give rise to numerous emerging applications of magnetic nanoparticles

P. Kuzhir
Institut de Physique de Nice (INPHYNI), CNRS UMR 7010, UCA, Parc Valrose, 06108 Nice cedex 2, France, e-mail: Pavel.Kuzhir@unice.fr

H. Ezzaier
Institut de Physique de Nice (INPHYNI), CNRS UMR 7010, UCA, Parc Valrose, 06108 Nice cedex 2, France, e-mail: ezzaier.hinda@gmail.com

J.A. Marins
Institut de Physique de Nice (INPHYNI), CNRS UMR 7010, UCA, Parc Valrose, 06108 Nice cedex 2, France, e-mail: jessica.alves-marins@inphyni.cnrs.fr

C. Magnet
Institut de Physique de Nice (INPHYNI), CNRS UMR 7010, UCA, Parc Valrose, 06108 Nice cedex 2, France, e-mail: Cecilia.Magnet@unice.fr

Y. Izmaylov
Institut de Physique de Nice (INPHYNI), CNRS UMR 7010, UCA, Parc Valrose, 06108 Nice cedex 2, France, e-mail: yaroslava.izmaylov@inphyni.cnrs.fr

C. Claudet
Institut de Physique de Nice (INPHYNI), CNRS UMR 7010, UCA, Parc Valrose, 06108 Nice cedex 2, France, e-mail: cyrille.claudet@inphyni.cnrs.fr

1 Introduction

Magnetic separation is a process in which magnetizable particles are extracted from a suspending liquid by means of magnetic field gradients. Apart from the classical application to ore beneficiation [1], magnetic separation has been finding new, emerging applications in water purification [2] and in the separation of living cells or biological molecules [3]. The basic idea is to attach pollutant molecules, biomolecules or cells to magnetic particles and extract them from the suspending liquid using an externally applied non-uniform magnetic field that creates a magnetic force on particles making them move in the direction of the magnetic field gradient. In most existing applications, magnetic micron-sized particles are used, providing an easy magnetic separation with moderate magnetic fields, while the use of nanoparticles is considered to be inefficient because of their strong Brownian motion. This is a real technological barrier for many biological and environmental applications because small nanoparticles have a high specific area and would capture larger amounts of molecules by unit suspension volume as compared to microbeads; this would allow either an enhancement of the biomolecule detection or reduction of the amount of reagents necessary for bioanalysis or water purification. Magnetic separation efficiency of nanoparticles is especially low in microfluidic devices relevant for most biomedical applications because it is difficult to realize high magnetic fields in a compact geometry of these devices.

However, a few years ago, we showed that the magnetic separation of nanoparticles can still be efficient if they undergo a field-induced phase separation manifested by appearance of long micron-sized needle-like aggregates containing millions of nanoparticles [4, 5]. The capture efficiency of such a phase separating system is related to the aggregate size scale rather than to the size of individual nanoparticles. To benefit from the phase separation to enhance the magnetic separation of nanoparticles, one needs to know: (a) the range of magnetic field intensity and nanoparticle concentration at which the phase separation takes place; (b) how fast the phase separation is in comparison to magnetic separation; (c) what is the optimal geometry of the magnetic separator providing a maximal capture efficiency of nanoparticles. These points impose a detailed study of (a) the phase separation equilibrium with establishment of the phase diagrams; (b) kinetics of field-induced nanoparticle aggregation; (c) capture of nanoparticles on magnetizable collectors of a microfluidic magnetic separator. In this paper, we briefly review these points and show how basic physical concepts allow designing a very efficient magneto-microfluidic separation system expected to give a considerable improvement of high sensitivity immunoassays.

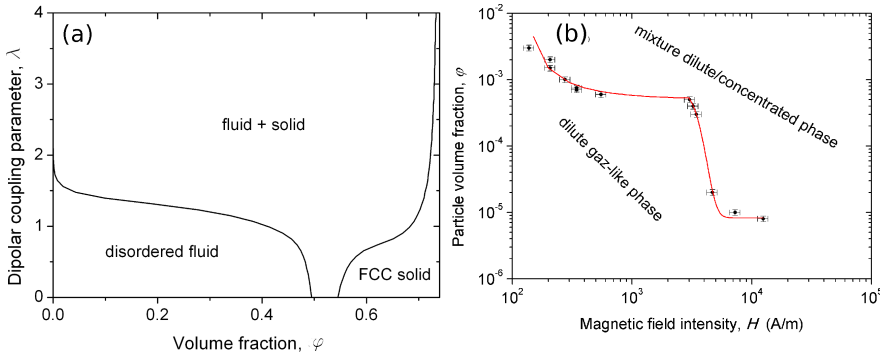

Fig. 1 Theoretical (a) and experimental (b) phase diagrams of a suspension of magnetizable nanoparticles showing diluted phase (disordered fluid), a concentrated phase (fcc solid) and a mixture of both phases (fluid + solid). Only one binodal curve is accessible in experiments and this curve corresponds to the onset of field-induced aggregation. (a) is reprinted from Magnet et al. Phys Rev E **89**, 032310 (2014) with kind permission of American Physical Society and (b) is reprinted from Ezzaier et al. J. Chem. Phys. **146**, 114902 (2017) with kind permission of American Institute of Physics.

2 Phase equilibrium

Let us consider a homogeneous suspension of Brownian magnetizable nanoparticles of a diameter d dispersed in a liquid. If this suspension is subjected to a uniform external magnetic field of an intensity H, the nanoparticles acquire a magnetic moment m and undergo dipolar interactions between them. If the particle concentration and the applied magnetic field are strong enough, the suspension will undergo a phase separation, i.e., the nanoparticles will form dense needle-like aggregates (concentrated phase) separated by a suspending liquid containing a small amount of particles (dilute phase). The phase separation is governed by two dimensionless parameters – the nanoparticle volume fraction φ and the dipolar coupling parameter λ defined as a ratio of the dipolar interaction energy to the thermal agitation energy $k_B T$:

$$\lambda \sim \frac{m^2}{\mu_0 k_B T d^3} \sim \frac{\mu_0 H^2 d^3}{k_B T}, \tag{1}$$

where $\mu_0 = 4\pi \times 10^{-7}$ H/m is the magnetic permeability of vacuum.

The dilute and concentrated phases, as well as their mixture, are mapped onto a λ-φ phase diagram shown in Fig. 1a with the boundaries between phases (binodal curves) calculated by equating chemical potentials and osmotic pressures in both phases [6].

As inferred from Fig. 1a, the dilute phase occupies the space below the left binodal curve, the concentrated phase is below the right binodal curve, while the mixture of two phases is between these curves. The left binodal curve shows at which critical dipolar coupling parameter (or, equivalently, critical magnetic field) the nanoparticles start to aggregate and thus bears the important information for the magneto-microfluidic separation (Sec. IV). This curve was also measured experimentally by direct optical observation of the aggregation of a nanoparticle suspension subjected to different external magnetic fields [7]. As nanoparticles, we used nanoclusters of a medium size of the order of 50 nm dispersed in water and composed of a dozen smaller iron oxide nanoparticles assembled by a double layer oleic acid surfactant [8]. The same nanoparticles have been used for all experiments presented in the current paper. The shape of the experimental binodal curve, shown in Fig. 1b, exhibits some similarities with the left binodal curve of Fig. 1a calculated theoretically. However, the theory underestimates the critical magnetic field of the onset of aggregation, likely because of attractive van der Waals interactions between nanoparticles ignored in the theory.

3 Kinetics of aggregation

The field-induced phase separation described in Sec. 2 has a certain timescale, important for a proper design of the magneto-microfluidic separation system. Experimentally, kinetics of phase separation or, equivalently, kinetics of nanoparticle aggregation has been studied by optical observation of a nanoparticle suspension sandwiched between two glass plates and subjected to an external magnetic field of a given intensity H [7]. Starting from some time elapsed from the moment of the magnetic field application, one observes appearance of black stripes aligned with the direction of the applied magnetic field and corresponding to bulk needle-like aggregates of a length of the order of a hundred of microns and a width of the order of a few microns. The effect of the particle volume fraction φ and of the applied magnetic field H on the aggregation state of the suspension is inspected in Fig. 2 where snapshots of the suspension microstructure are shown at a given elapsed time $t = 20$ min but for different φ and H. As expected, the aggregate length and thickness seem to increase significantly with increasing magnetic field and particle concentration thanks to enhancement of magnetic interactions between nanoparticles.

To quantify the kinetics of aggregation, the time dependence of the aggregate average length L is inspected in Fig. 3 for the magnetic field intensity $H = 2.75$ kA/m and for three different particle volume fractions. The experi-

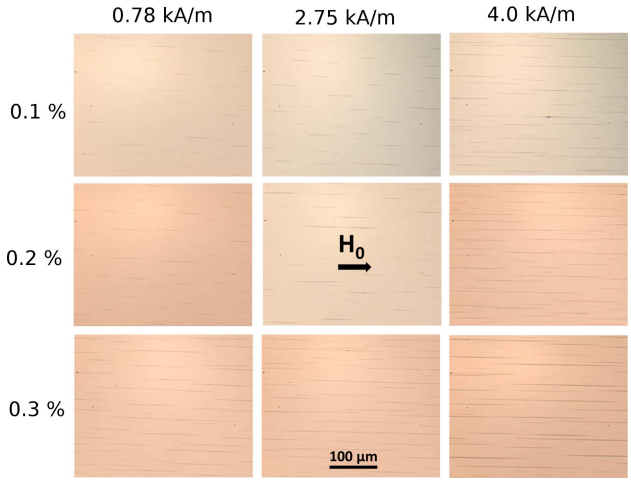

Fig. 2 Snapshots of the suspension microstructure at the fixed elapsed time $t = 20\,\text{min}$ and different intensities H (or H_0) of the applied magnetic field and different particle volume fractions φ (reprinted from Ezzaier et al. J. Chem. Phys. **146**, 114902 (2017) with kind permission of American Institute of Physics).

mental curves show an initial sublinear increase of the aggregate length with time, followed by a change in the slope at $t \approx 10 - 15\,\text{min}$ and by a stronger increase. From the theoretical point of view, a stage of aggregate growth (by diffusion and magnetophoretic migration of nanoparticles towards primary nuclei) is expected at shorter times providing a sublinear section of $L(t)$-dependency, while a coalescence regime (merging of aggregates due to their dipole-dipole interaction) is expected at longer times providing a stronger than linear increase of the aggregate size. Transition between two regimes is supposed to take place when the aggregation rate of the coalescence stage becomes larger than that of the aggregate growth stage; such a transition results in a change of the slope of the $L(t)$-curves. Our theoretical model (solid curves on Fig. 3) fits at least semi-quantitatively to the experiments. As inferred from the figure inset, the change of the slope is predicted at higher elapsed times than those observed in experiments.

The most important issues for magnetic separation (Sec. 4) are the timescales t_G and t_C of the aggregate growth and coalescence stages, respectively:

$$t_G \sim \frac{d^2}{D_n \Delta_0} \left(\frac{V_m}{d^3} \right)^{4/7}; \qquad t_C \sim \frac{\eta}{\Phi \mu_0 M^2}, \tag{2}$$

where D_n is the nanoparticle diffusion coefficient; $\Delta_0 = \varphi - \varphi\prime(\lambda)$ is the initial supersaturation of the suspension corresponding to the difference of the

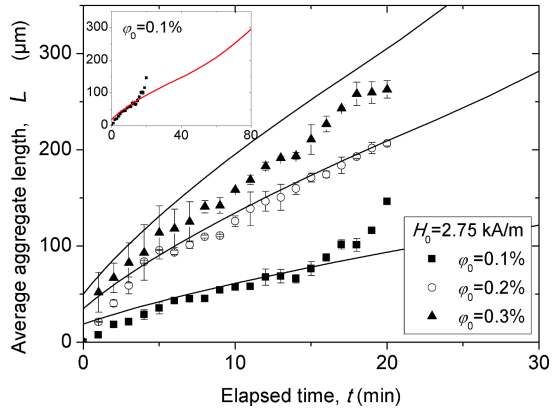

Fig. 3 Experimental (symbols) and theoretical (lines) dependencies of the average aggregate length on elapsed time for the applied magnetic field $H = 2.75\,\mathrm{kA/m}$ at different particle volume fractions. The inset shows the same dependency for $\varphi = 0.1$ vol.% in an extended timescale (reprinted from Ezzaier et al. J. Chem. Phys. **146**, 114902 (2017) with the kind permission of the American Institute of Physics).

particle volume fraction and the critical volume fraction $\varphi\prime(\lambda)$ at the onset of aggregation (left binodal curve on Fig. 1a or the curve on Fig. 1b); V_m is the maximum aggregate volume in the aggregate growth regime corresponding to vanishing supersaturation; η is the suspending liquid viscosity; M and Φ are the magnetization of aggregates and their volume fraction in the suspension, respectively. Both estimations using Eq. 2 and experiments show that the shortest timescale giving the aggregate length of the order of 10 μm is about 1 min. Thus, we have to design the magnetic separation system in such a way that the particle traveling time has to be larger than $t \sim 1$ min such that the nanoparticles have enough time to aggregate under the action of the applied field.

4 Magnetic separation

Ordered arrays of magnetizable micropillars are considered to be one of the most effective geometries for the separation of magnetic micron sized particles in microfluidic scale [9, 10]. We have shown that such system provides an acceptable capture efficiency of magnetic nanoparticles undergoing field-induced aggregation [4]. A sketch of a microscale channel equipped with an array of nickel micropillars is presented in Fig. 4. Micropillar arrays were grown on a glass substrate by electroplating and soft photolithography. In experiments an aqueous suspension of iron oxide nanoparticles of a desired concentration φ was pushed through the channel at a desired speed u using

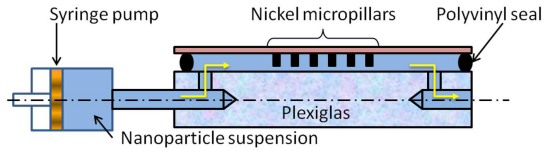

Fig. 4 Microfluidic channel with a micropillar array (reprinted from Ezzaier et al. J. Magn. Magn. Mater. **459**, 350 (2018) with the kind permission of Elsevier)

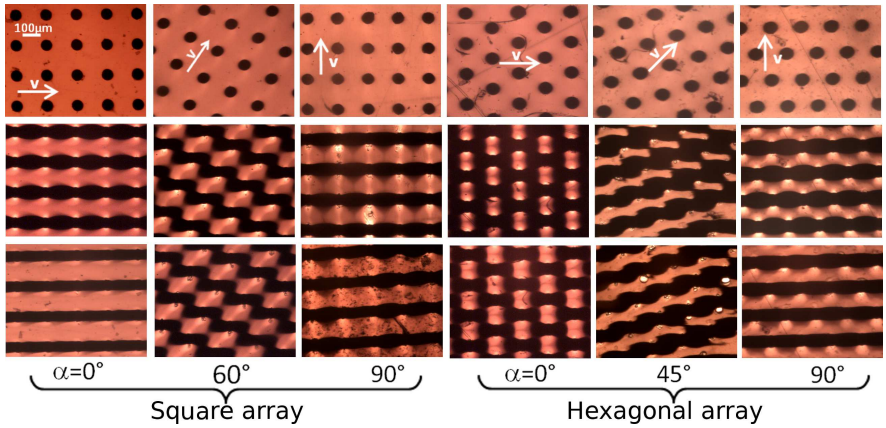

Fig. 5 Snapshots of nanoparticle deposits around micropillars (reprinted from Ezzaier et al. J. Magn. Magn. Mater. **459**, 350 (2018) with the kind permission of Elsevier)

a syringe pump and in the presence of an external magnetic field of a given intensity H.

Once the field was applied, the nickel micropillars became magnetized and started to attract magnetic nanoparticles and separate them from the suspending liquid (water) building particle deposits around the micropillars. Snapshots of nanoparticle deposits were recorded over time and some of them are shown in Fig. 5. The upper row of snapshots shows the top view of the micropillar arrays without captured nanoparticles, the middle and the bottom rows show nanoparticle deposits at the flow speed $u = 0.71\,\mathrm{mm/s}$ and $2.14\,\mathrm{mm/s}$, respectively, at an applied magnetic field $H = 13.5\,\mathrm{kA/m}$, nanoparticle volume fraction $\varphi = 0.3$ vol.% and elapsed time $t = 60\,\mathrm{min}$. Different columns correspond to different directions between the flow and the magnetic field, characterized by an angle α. Qualitatively, the flow intensity and orientation influence the shape of the deposits that evolve to a straight pattern with increasing speed in the case of a square array with $\alpha = 0^\circ$ [bottom left snapshot in Fig. 5] or to honeycomb pattern in the case of hexagonal array at $\alpha = 0^\circ$ [4^{th} column from the left on Fig. 5].

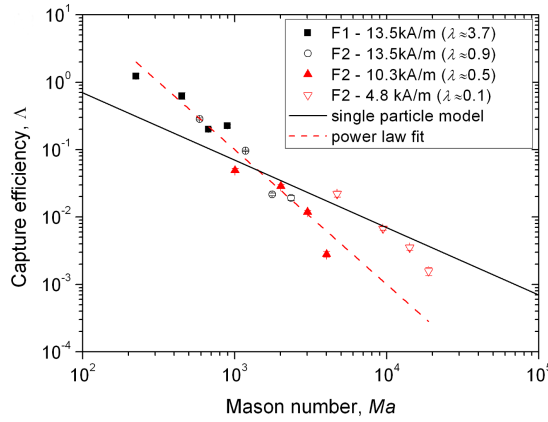

Fig. 6 Mason number dependency of the capture efficiency at different dipolar coupling parameters λ and fixed values of $\varphi = 0.3\%$, $\alpha = 0^\circ$ and for the square array (reprinted from Ezzaier et al. J. Magn. Magn. Mater. **459**, 350 (2018) with the kind permission of Elsevier).

Quantitatively, experimental dependencies of the deposit area S on elapsed time t were obtained by image processing of the snapshots. The slope of the experimental $S(t)$ curves was related to the capture efficiency – the key parameter characterizing the separation performance – defined as $\Lambda = \ln(\varphi_{in}/\varphi_{out})$, with $\varphi_{in} = \varphi$ and φ_{out} being the nanoparticle volume fractions at the channel inlet and outlet respectively [11]. It has been shown that the most important parameter affecting the capture efficiency is the Mason number, defined as the ratio of hydrodynamic to magnetic forces acting on nanoparticles:

$$\mathrm{Ma} = \frac{6\eta u D}{\beta \mu_0 H^2 d^2}, \tag{3}$$

where $D = 50\,\mu$m is the micropillar diameter and $\beta \approx 0.9$ is the magnetic contrast factor of nanoparticles. Mason number dependency of the capture efficiency *Lambda* is plotted in Fig. 6 for three different values of the applied magnetic fields H and two different average diameters d of nanoparticles (samples F1 with $d = 68$ nm and F2 with $d = 42$ nm).

Variations of d and H result in a variation in the dipolar coupling parameter [Eq. 1] in the range $0.1 \leq \lambda \leq 3.7$. Three experimental Λ versus Ma curves, corresponding to $\lambda \leq 0.5$, are gathered along a straight line in log-log scale and fitted by a scaling law $\Lambda \propto \mathrm{Ma}^{-2}$ (dashed line on Fig. 6), while the fourth curve with $\lambda \approx 0.1$ shows a weaker Mason number dependency. Experiments show that nanoparticle suspensions undergo phase separation with appearance of bulk aggregates at $\lambda \geq 0.5$ and $\varphi = 0.3\%$. Intense shear flows around the micropillars can disrupt nanoparticles from aggregates such that the aggregate size is expected to be a decreasing function of the Mason number. The combination of this effect with increasing convective

flux transporting the aggregates could explain a strong decrease of the capture efficiency with Mason number ($\Delta \propto \mathrm{Ma}^{-2}$) for $\lambda \geq 0.5$. Our theoretical model predicts a quite similar behavior ($\Delta \propto \mathrm{Ma}^{-1.7}$) [4]. Notice that in the considered range of the Mason numbers, the nanoparticle travel time is typically larger than the aggregation timescale $\tau \sim 1$ min estimated in Sec. 3. This leaves enough time to the nanoparticle to form micron-sized aggregates that are efficiently captured by micropillars. However, nanoparticle suspensions do not exhibit phase separation at λ=0.1 and $\varphi = 0.3\%$. In this case, the capture efficiency of individual nanoparticles is only defined by a compromise between convective and magnetophoretic fluxes resulting in a theoretical scaling law $\Delta \propto \mathrm{Ma}^{-1}$ [4] (solid line on Fig. 6), which fits reasonably well to experimental points for λ=0.1 (triangles on Fig. 6). The effects of the particle concentration, magnetic field orientation and array geometry (square or hexagonal) are analysed in details in [11].

5 Conclusions

In this work, we have briefly reviewed magnetic separation of nanoparticles on a microfluidic scale. In the presence of an applied uniform magnetic field, the nanoparticle suspension may undergo a phase separation, fully governed by the particle volume fraction φ and the dipolar coupling parameter λ and accompanied by appearance of bulk needle-like aggregates. Such field-induced aggregation strongly enhances the capture efficiency of magnetic particles on ordered arrays of magnetizable micropillars, especially if the particle traveling time is larger than the aggregation timescale. The capture of such aggregates by micropillars depends mostly on the ratio of hydrodynamic-to-magnetic forces: the Mason number. Besides this, tuning the array's geometry and magnetic field orientation allows for the generation of particular patterns of nanoparticle deposits around the micropillars minimally affected by the flow and providing a maximized retention capacity. This could be useful for development of microscale magnetic separators for biomedical applications. In particular, we are currently working on nanoparticle-based magneto-microfluidic immunoassays with enhanced sensitivity.

We acknowledge the financial support of French government piloted by ANR in framework of the Future Investments UCA$^{\mathrm{JEDI}}$ project, ANR-15-IDEX-01.

References

1. Svoboda J.: Magnetic Techniques for the Treatment of Materials, Kluwer Academic, Dordrecht (2004)
2. Ambashta R.D., Sillanpää M.: Water purification using magnetic assistance: A review, J. Hazardous Materials **180**, 38 (2010)
3. Zborowski M., Chalmers J.J.: Magnetic cell separation, Elsevier, Amsterdam (2008)
4. Orlandi G., Kuzhir P. , Izmaylov Y., Marins J. A., Ezzaier H., Robert L., Doutre F., Noblin X., Lomenech C., Bossis G., Meunier A., Sandoz G., and Zubarev A.: Microfluidic separation of magnetic nanoparticles on an ordered array of magnetized micropillars Phys. Rev. E **93**, 062604 (2016)
5. P. Kuzhir, C. Magnet, H. Ezzaier, A.Zubarev, G.Bossis: Magnetic filtration of phase separating ferrofluids: From basic concepts to microfluidic device J. Magn. Magn. Mater. **431**, 84 (2017).
6. C. Magnet, P. Kuzhir, G. Bossis, A. Meunier, S. Nave, A. Zubarev, C. Lomenech, and V. Bashtovoi: Behavior of nanoparticle clouds around a magnetized microsphere under magnetic and flow fields Phys. Rev. E **89** 032310 (2014).
7. Ezzaier H., Alves Marins J., Razvin I., Abbas M., Ben Haj Amara A., Zubarev A., Kuzhir P.: Two-stage kinetics of field-induced aggregation of medium-sized magnetic nanoparticles J. Chem. Phys. **146**, 114902 (2017).
8. Magnet C., Kuzhir P., Bossis G., Meunier A., Suloeva L., Zubarev A.: Haloing in bimodal magnetic colloids: The role of field-induced phase separation Phys. Rev. E **86** 011404 (2012).
9. Deng T., Prentiss M., Whitesides G.M.: Fabrication of magnetic microfiltration systems using soft lithography Appl. Phys. Lett. **80**, 461 (2002)
10. Palfreyman J.J., van Belle F. , Lew W.-S., Mitrelias T., Bland J. A. C., Lopalco M., Bradley M.: Hybridization of Electrodeposited Magnetic Multilayer Micropillars IEEE Trans. Magn. **43**, 2439 (2007)
11. Ezzaier H.,Marins J. A., Schaub S., Amara B. H., Kuzhir P.: Capture of magnetic nanoparticles on ordered magnetizable arrays: A parametric study J. Magn. Magn. Mater. **459**, 350 (2018)